Origin of Ferrimagnetism and Ferroelectricity in Room-Temperature Multiferroic ε-Fe_2O_3

K. Xu,[1,2,3] J. S. Feng,[1,3,5] Z. P. Liu,[4,*] and H. J. Xiang[1,3,†]

[1]*Key Laboratory of Computational Physical Sciences (Ministry of Education), State Key Laboratory of Surface Physics, and Department of Physics, Fudan University, Shanghai 200433, People's Republic of China*

[2]*Hubei Key Laboratory of Low Dimensional Optoelectronic Materials and Devices, Hubei University of Arts and Science, Xiangyang 441053, People's Republic of China*

[3]*Collaborative Innovation Center of Advanced Microstructures, Nanjing 210093, People's Republic of China*

[4]*Collaborative Innovation Center of Chemistry for Energy Material, Shanghai Key Laboratory of Molecular Catalysis and Innovative Materials, Key Laboratory of Computational Physical Science (Ministry of Education), Department of Chemistry, Fudan University, Shanghai 200433, China*

[5]*School of Electronic and Information Engineering, Hefei Normal University, Hefei 230601, China*

(Received 18 May 2017; revised manuscript received 11 December 2017; published 9 April 2018)

Exploring and identifying room-temperature multiferroics is critical for developing better nonvolatile random-access memory devices. Recently, ε-Fe_2O_3 was found to be a promising room-temperature multiferroic with a large polarization and magnetization. However, the origin of the multiferroicity in ε-Fe_2O_3 is still puzzling. In this work, we perform density-functional-theory calculations to reveal that the spin frustration between tetrahedral-site Fe^{3+} spins gives rise to the unexpected ferrimagnetism. For the ferroelectricity, we identify a low-energy polarization switching path with an energy barrier of 85 meV/f.u. by performing a stochastic surface walking simulation. The switching of the ferroelectric polarization is achieved by swapping the tetrahedral Fe ion with the octahedral Fe ion, different from the usual case (e.g., in $BaTiO_3$ and $BiFeO_3$) where the coordination number remains unchanged after the switching. Our results not only confirm that ε-Fe_2O_3 is a promising room-temperature multiferroic but also provide guiding principles to design high-performance multiferroics.

DOI: 10.1103/PhysRevApplied.9.044011

I. INTRODUCTION

Multiferroic materials, which simultaneously possess more than two ferroic orderings, have attracted tremendous attention recently [1–6]. Cross-control between magnetism and ferroelectricity in a compound (single crystal) with little energy dissipation is a promising merit that combine fast electrical writing and magnetic reading for developing the next generation of information storage, sensing devices, etc. [7,8]. To this end, finding room-temperature multiferroics with strong polarization and large magnetization is desirable [9]. At present, the perovskite-type bismuth ferrite $BiFeO_3$ (BFO) is the most well-known room-temperature multiferroic material. It remains ferroelectric up to $T_C = 1100$ K with a large saturated polarization of 100 $\mu C\,cm^{-2}$. However, below $T_N = 640$ K, bulk BFO exhibits an antiferromagnetic- (AFM) like incommensurate cycloidal-type spin configuration [10], which leads to zero net magnetization and hinders its realistic applications.

Interestingly, ε-Fe_2O_3 was discovered to be a room-temperature multiferroic with strong ferrimagnetism and ferroelectricity [11]. Together with the fact that it contains only inexpensive and nontoxic elements, ε-Fe_2O_3 is a promising candidate for making novel memory devices. As shown in Fig. 1(a), ε-Fe_2O_3 adopts a polar orthorhombic structure with the $Pna2_1$ space group [12]. The 16 Fe^{3+} ions in a unit cell can be divided into four different sublattices labeled *A*, *B*, *C*, and *D*. Among them, the *A* and *B* sublattices are two distorted octahedral sites, the *C* sublattice is a regular octahedral site, while the *D* sublattice is a tetrahedral site. As early as 1963, Schrader and Büttner reported that ε-Fe_2O_3 was a robust room-temperature insulating ferrimagnet with a high Curie temperature of about 500 K [13]. Up to now, the magnetic structure of ε-Fe_2O_3 at room temperature has not been completely determined. Different magnetic structures such as antiferromagnetic alignment [14] and noncollinear ferrimagnetic alignment [12] were reported in early studies. A later experiment suggested a collinear spin arrangement [see Figs. 1(a) and 1(b)] for the ferrimagnetic state at room

*zpliu@fudan.edu.cn
†hxiang@fudan.edu.cn

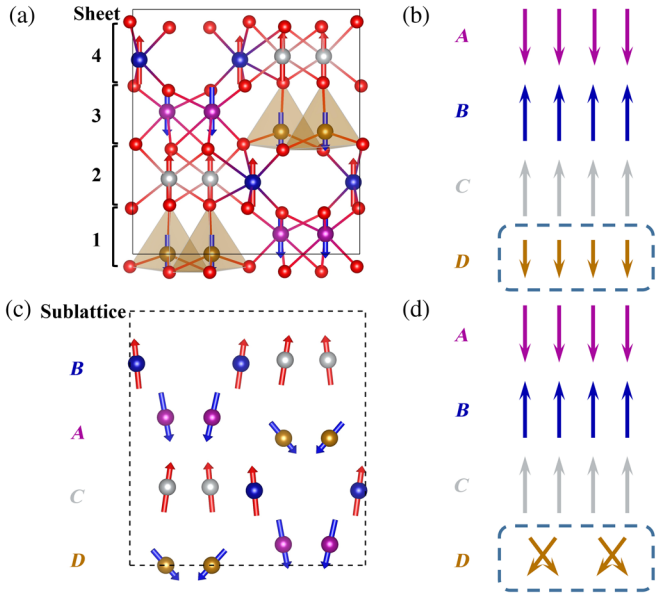

FIG. 1. Structure and spin configurations in ε-Fe_2O_3. (a) Perspective view of ε-Fe_2O_3 crystal structure along the [100] direction. There are four Fe sublattices, namely, octahedral sites Fe-*A*, Fe-*B*, Fe-*C*, and the tetrahedral site Fe-*D*, which are displayed in purple, blue, silver, and yellow, respectively. ε-Fe_2O_3 can be viewed as a layered structure, and each sheet contains two sublattices of Fe^{3+} ions. (b) The suggested experimental magnetic structure [also shown in (a)] in ε-Fe_2O_3 at room temperature. The nonzero net magnetization of this collinear magnetic structure is due to the smaller magnetic moment of group-*D* Fe^{3+} cations. (c),(d) The lowest-energy magnetic structure from our MC simulation. In this magnetic structure, the four Fe^{3+} sublattices have almost the same local magnetic moment. The nonzero net magnetization of this noncollinear magnetic structure is due to the fact that the spin directions of two adjacent *D*-sublattice Fe^{3+} ions are nearly perpendicular to each other. Oxygen atoms are not shown in (b)–(d).

temperature with a net magnetization of $0.3\mu_B$ per Fe^{3+} [15]. This magnetic structure can be viewed as an AFM stacking of four ferromagnetic (FM) spin sheets [1–4 in Fig. 1(a)]. It was speculated that the local magnetic moment of the tetrahedral *D* sublattice is much smaller than those of the other three octahedral sublattices, resulting in a net magnetization. However, the local magnetic moment of the high-spin Fe^{3+} ion should be close to $5\mu_B$ in both a tetrahedral and octahedral coordination environment, which was verified both experimentally and theoretically [16,17]. For the closely related compound iron oxide $Bi_2Fe_4O_9$, which also contains FeO_4 tetrahedra and FeO_6 octahedra, the neutron-diffraction measurements show that the magnetic moment per Fe^{3+} ion for both tetrahedral and octahedral sites is about $4.95 \pm 0.08\mu_B$ [16], and density-functional-theory (DFT) calculations indicate that the local spin moment for each Fe^{3+} ion ($S = 5/2$) in $Bi_2Fe_4O_9$ is close to $5\mu_B$, as expected [17]. Therefore, a complete understanding of the mechanism of the ferrimagnetism is still missing.

Regarding the ferroelectricity in ε-Fe_2O_3, the recent discovery that ε-Fe_2O_3 thin film exhibits switchable ferroelectric polarization under a small voltage (approximately 1 V) [11] is also surprising and puzzling. It is well known that to be a ferroelectric (FE), the polar system should be switchable by an electric field (otherwise, it is only a piezoelectric). To be switchable by an electric field, the potential barrier [i.e., the energy difference between the paraelectric (PE) state and FE state] should be small enough. For example, polar wurtzite ZnO is not a switchable ferroelectric because the energy barrier is as high as 0.25 eV/f.u. [18]. The finding that ε-Fe_2O_3 is a switchable ferroelectric is surprising because a very high-energy barrier (0.6–1.3 eV/f.u.) was predicted in an isostructural compound $GaFeO_3$ with the same space group $Pna2_1$ [19,20]. Therefore, it is not clear why the electric polarization in ε-Fe_2O_3 can be switched. Understanding the microscopic origins of the ferrimagnetism and ferroelectricity in ε-Fe_2O_3 is not only scientifically important, but it also helps to improve the multiferroic properties of ε-Fe_2O_3 and related materials.

In this work, we combine first-principles calculations, parallel tempering Monte Carlo (PTMC) simulation, and a stochastic surface walking approach to explore the origin of ferrimagnetism and ferroelectricity in ε-Fe_2O_3. Although the experimentally proposed collinear AFM state is confirmed to have the lowest energy among all the possible collinear magnetic configurations, our PTMC simulation shows that the lowest magnetic state is noncollinear with the magnetic moments of two adjacent Fe^{3+} ions in the *D* sublattice nearly perpendicular to each other. Finally, a low-energy paraelectric state with the *Pbcn* space group is predicted from the stochastic surface walking (SSW) simulation. The energy barrier for the FE switching is about 85 meV/f.u., which is much smaller than the previously suggested value (0.6–1.3 eV/f.u.) for the related compound $GaFeO_3$.

II. RESULTS AND DISCUSSION

A. Finding the lowest energy of collinear spin configuration in ε-Fe_2O_3

We first check whether the proposed experimental collinear spin structure [Figs. 1(a) and 1(b)] indeed has low energy. As we mention above, ε-Fe_2O_3 has four different sublattices. Each sublattice contains four Fe^{3+} ions at the 4*a* Wyckoff positions. It can be seen as a layered structure with four Fe^{3+} sheets [1–4 in Fig. 1(a)]. By symmetry, sheet 1 (respectively, 2) is equivalent to sheet 3 (respectively, 4). Since ε-Fe_2O_3 has 16 Fe^{3+} in a unit cell, there are 2^{16} collinear spin configurations in total. When taking into account the space group and time-reversal symmetries, the number of inequivalent collinear spin

configurations is reduced to 8384. We perform DFT calculations on all inequivalent 8384 configurations (see Supplemental Material in Ref. [21], Fig. S1) to find out the lowest-energy collinear spin configuration. Our DFT results show that this collinear lowest-energy state adopts an intrasheet FM coupling and intersheet AFM coupling, in accordance with the experimental results. The DFT + U calculations demonstrate that the collinear configuration has an exact zero total magnetic moment. This can be understood since all the high-spin Fe^{3+} ions have local moments close to $5\mu_B$, and the total spin magnetic moment per cell must be an integer in an insulating system. Additional DFT + U + SOC calculations show that the orbital magnetic moments are very small (approximately $0.02\mu_B$/Fe) for the Fe^{3+} d^5 ion. These results suggest that the real magnetic state at room-temperature ε-Fe_2O_3 should not be the collinear spin configuration as proposed before.

B. Magnetic interactions in ε-Fe_2O_3

In order to find out a more reasonable magnetic structure for ε-Fe_2O_3, we calculate all the relevant Heisenberg interaction parameters. Since the unit cell of ε-Fe_2O_3 is large and the symmetry is low, the spin interactions in ε-Fe_2O_3 are rather complicated. By virtue of the fact that the Heisenberg exchange interaction is short ranged, we calculate only the interaction between pairs for which the distance does not exceed 6 Å. In total, there are 60 Fe-Fe pair interactions, including 23 Fe—O—Fe superexchange interactions and 37 Fe—O···O—Fe super-superexchange interactions. All the super-super-exchange parameters are found to be smaller than 2.6 meV, which are hereafter disregarded. All the superexchange interactions are found to be of the AFM nature (see Ref. [21], Table S1). The symmetry of the $Pna2_1$ space group guarantees that the intersheet interaction between 1 and 2 and between 3 and 4 is equivalent (similarly, the 2-3 interaction is equivalent to the 1-4 interaction). Thus, we need to calculate only the intersheet 1-2 interaction and the intersheet 2-3 interaction. The 16 important superexchange paths labeled as $\boldsymbol{J}_5$, $\boldsymbol{J}_6$ (intrasheet interactions) and $\boldsymbol{J}_8$ to $\boldsymbol{J}_{21}$ (intersheet interactions) are displayed in Fig. 2. The complete superexchange paths and their magnitude are shown in Ref. [21], Fig. S2 and Table S1.

With these calculated spin-exchange parameters, we are now in a position to discuss the magnetic ground state. We can see that the intrasheet exchange interactions are weaker than the intersheet exchange interactions: The sums of the intersheet exchange interactions between sheets 1 and 2 and between sheets 2 and 3 are 656.50 and 478.09 meV, respectively, while the sums of the intrasheet exchange interactions for sheets 1 and 2 are 207.58 and 28.86 meV, respectively. This suggests that the magnetic structure is mainly determined by the intersheet interactions.

Let us consider which magnetic structure has the lowest energy if only the intersheet interactions are taken into account. The C-sublattice Fe ion in the second sheet simultaneously interacts with two D-sublattice Fe ions in sheet 1 through $\boldsymbol{J}_8$ and $\boldsymbol{J}_9$. Since both $\boldsymbol{J}_8$ and $\boldsymbol{J}_9$ are AFM, the spin directions of two D-sublattice Fe ions must be opposite to that of the C-sublattice Fe ion. As a result, the intrasheet spin alignment within sheet 1 and sheet 2 is ferromagnetic, while the intersheet spin alignment between sheet 1 and sheet 2 is AFM. For the other intersheet interactions, a similar analysis can be applied. Therefore, when considering only the intersheet interactions, we find that ε-Fe_2O_3 adopts the intrasheet FM coupling and intersheet AFM coupling, similar to the A-type spin order in perovskite systems and the experimentally suggested magnetic configuration.

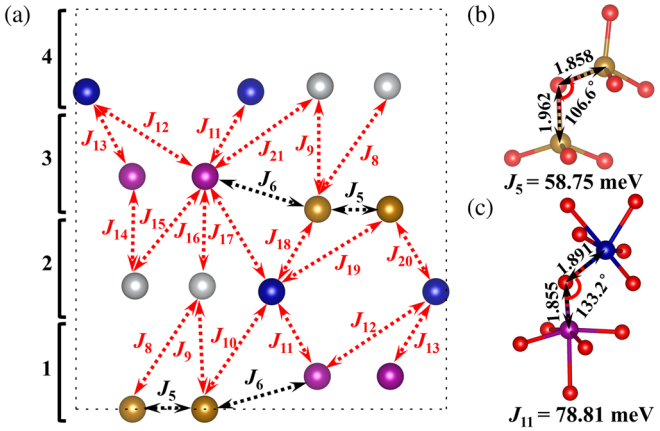

FIG. 2. Spin-exchange interactions in ε-Fe_2O_3. (a) Strong superexchange paths in ε-Fe_2O_3. All superexchange interactions are found to be AFM. $\boldsymbol{J}_5$ and $\boldsymbol{J}_6$ are intrasheet interactions, while $\boldsymbol{J}_8$ to $\boldsymbol{J}_{21}$ are the intersheet interactions. For clarity, the intrasheet and intersheet interactions are black and red, respectively. The intersheet interactions are much stronger than the intrasheet interactions in most cases. The AFM intersheet interactions lead to the intersheet AFM coupling and intrasheet FM coupling. The exchange interaction ($\boldsymbol{J}_5$) between the two neighboring D-sublattice Fe sites is the strongest among all intrasheet interactions, which leads to a spin frustration (see the triangle composed by $\boldsymbol{J}_5$, $\boldsymbol{J}_8$, and $\boldsymbol{J}_9$). (b),(c) The local environment for the strongest intrasheet interaction ($\boldsymbol{J}_5$) and strongest intersheet interaction ($\boldsymbol{J}_{11}$). The Fe—O—Fe bond angles and Fe—O bond lengths are indicated.

The collinear magnetic structure might be disturbed by the intrasheet interactions. The strongest intrasheet interaction ($\boldsymbol{J}_5 = 58.75$ meV) is between the D-D Fe^{3+} pair within sheet 1, which is smaller but still not negligible when compared with the strongest intersheet interaction ($\boldsymbol{J}_{11} = 78.81$ meV between the A-D Fe^{3+} pair). The relative magnitude of the exchange interactions can be understood within the Goodenough-Kanamori rule [32]. These two superexchange interactions are mediated by the corner-sharing oxygen atoms; see Figs. 2(b) and 2(c). For the D-D pair, the average Fe—O bond length and bond angle are 1.91 Å and 107°, respectively; for the A-D pair,

the average Fe—O bond length and bond angle are 1.85 Å and 133°, respectively. The magnitudes of the superexchange parameters $\boldsymbol{J}_5$ and $\boldsymbol{J}_{11}$ are proportional to the Fe—O—Fe bond angle and inversely proportional to the Fe—O bond length, in accordance with the Goodenough-Kanamori rule [32]. The significant intrasheet *D*-*D* exchange interaction ($\boldsymbol{J}_5$) is expected to change the magnetic structure due to the presence of a strong spin frustration, which can be easily seen from the triangle composed by the AFM $\boldsymbol{J}_5$, $\boldsymbol{J}_8$, and $\boldsymbol{J}_9$ interactions.

C. Spin-frustration-induced ferrimagnetism

Tronc *et al.* suggested nearly collinear ferrimagnetic order at the octahedral sites and lack of alignment with possible disorder at the tetrahedral sites [12]. To find the magnetic ground state in ε-Fe_2O_3, we perform a MC simulation in a $1 \times 1 \times 1$ cell at a low temperature (approximately 5 K). All superexchange interactions are taken into account. The lowest-energy configuration turns out to be noncollinear, as shown in Figs. 1(c) and 1(d). For each sublattice, the magnitude of the magnetic moments is nearly $5\mu_B$ per Fe^{3+} ion. We find that the spin correlation $\langle S_{D1}S_{D2}\rangle$ for the neighboring *D*-*D* Fe pair ($\boldsymbol{J}_5$) is nearly zero, indicating that the frustration is partially relieved by aligning the two spins perpendicular to each other. In addition, it is interesting to note that the angle between two adjacent *A* and *D* spins in the same sheet is nearly $\pi/3$ due to another intrasheet AFM interaction $\boldsymbol{J}_6$ (see Ref. [21], Fig. S2 and Table S1). For the other three sublattices (i.e., *A*, *B*, *C*), all spins are approximately parallel. Therefore, the magnetizations of the four sublattices are not completely canceled out, which induces a net magnetization (i.e., ferrimagnetism). Our DFT calculation shows that the noncollinear configuration indeed has a lower energy by 60 meV/f.u. than the experimentally suggested collinear configuration. We note that the noncollinear magnetic configuration is related to the experimentally suggested collinear magnetic configuration in two aspects: (1) The magnetic configuration of the *A*, *B*, *C* sublattices is almost the same, and (2) the moment of the *D* sublattice along the net magnetization direction is smaller than other sublattices in the noncollinear magnetic configuration despite the magnitude of the local moment of the *D* sublattice being the same as other sublattices. In contrast, the local moment of the *D* sublattice is smaller than other sublattices in the experimentally suggested collinear magnetic configuration.

The thermodynamic properties of ε-Fe_2O_3 are evaluated through the PTMC simulation with the $4 \times 4 \times 4$ supercell. Qualitatively similar results are obtained if a larger supercell (i.e., $8 \times 8 \times 8$ supercell) is adopted. The spin Hamiltonian contains Heisenberg symmetric exchange interactions. In Fig. 3(a), the specific heat C_v has a peak located at 483 K. The abrupt change of specific heat indicates that there is a magnetic phase transition around 483 K, which is very close to the experimental value (500 K) [11]. The average magnetic moment is about $0.28\mu_B$ per Fe at 200 K, which agrees nicely with the experimental magnetization of $0.3\mu_B$ per Fe^{3+} [15]. We define an order parameter $\vec{L}$ to characterize the AFM order of the system: $\vec{L} \sim \vec{M}_B + \vec{M}_C - \vec{M}_A - \vec{M}_D$. We find that $|\vec{L}|$ is smaller than $5\mu_B$/Fe, suggesting that the spins are not fully collinear. The temperature-dependent correlation functions $\chi(S_i, S_j; T) \sim \langle S_i S_j \rangle_T$ are calculated to further

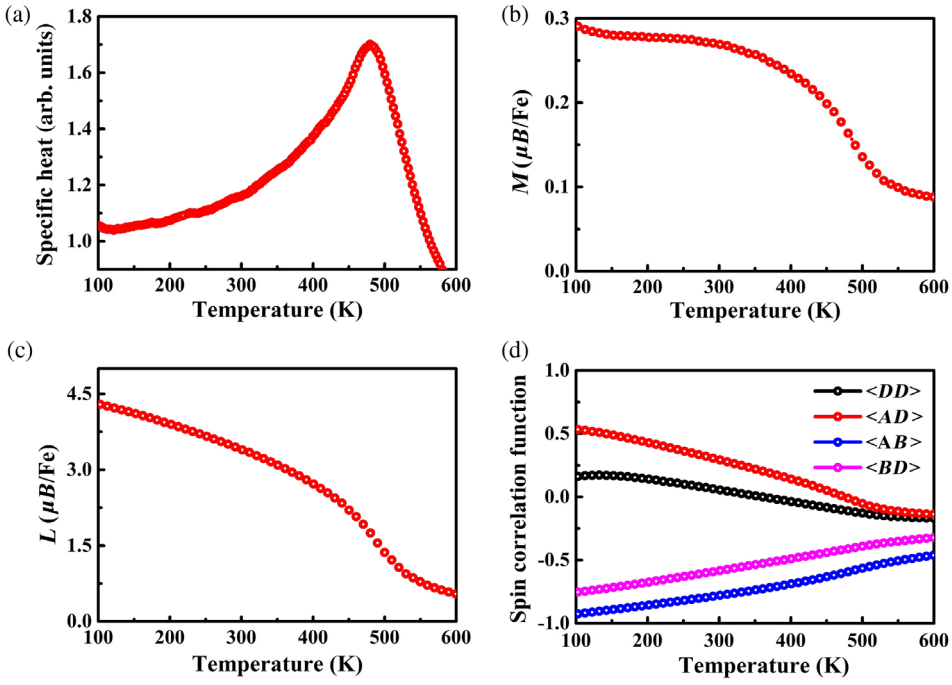

FIG. 3. Physical quantities from the PTMC simulations. (a) The specific heat C_v indicates that the ferrimagnetic-paramagnetic phase transition occurs at the Curie temperature (T_c) 483 K. (b) The average spin moment M shows that ε-Fe_2O_3 has a net magnetization of about $0.3\mu_B$/Fe. (c) The AFM order parameter L. (d) Spin correlation functions ($\langle S_i S_j \rangle$) for different Fe-Fe pairs. Spin correlation functions approach zero in the high-temperature paramagnetic state.

confirm the spin noncollinearity, as shown in Fig. 3(d). The correlation functions $\langle S_{D1}S_{D2}\rangle$ and $\langle S_A S_D\rangle$ are positive but smaller than 1, indicating the noncollinearity spin configurations between the *D*-*D* pair and *A*-*D* pair at room temperature. The correlation functions for the *A*-*B* and *B*-*D* pairs are nearly −1, suggesting that the spins are almost antiparallel to each other. At very high temperature, the magnitudes of the four correlation functions are nearly zero due to the randomness of the spin orientation, as expected. In conclusion, we demonstrate that the high-temperature ferrimagnetism in ε-Fe_2O_3 is due to the noncollinear spin canting. Different from the usual case where the spin frustration causes AFM ordering [33,34], here we reveal the spin frustration induced a strong ferrimagnetism in ε-Fe_2O_3.

D. SSW method predicting a transition state in ε-Fe_2O_3

After explaining the origin of the ferrimagnetism, we now turn to another puzzling issue, i.e., the ferroelectricity in ε-Fe_2O_3. The ε-Fe_2O_3 thin film was discovered to be a multiferroic material with a switchable polarization [10]. For the isostructural $GaFeO_3$ compound, a PE structure with the P*nna* space group was proposed. Mukherjee *et al.* [19] and Stoeffler [35] suggest that this P*nna* PE $GaFeO_3$ structure has a higher energy by 0.6 and 1.3 eV/f.u. than the P$na2_1$ FE $GaFeO_3$ structure, respectively. Our test calculation gives an energy barrier of 500 meV/f.u. for $GaFeO_3$, close to Mukherjee's result. For ε-Fe_2O_3, we find the P*nna* PE structure has a higher energy by approximately 340 meV/f.u. than the P$na2_1$ FE structure (see Ref. [21], Figs. S4 and S5). Such a large energy difference between the P*nna* PE structure and the P$na2_1$ FE structure suggests that the P*nna* PE structure is questionable.

To find a more reasonable PE structure, the first-principles-based SSW simulation for finding the switching path [36] is performed. Our SSW method is applied successfully to describe the solid-state phase transition in rutile and 2D δ-MnO_2, etc. [36,37]. Using this method, we predict a low-energy PE state with the P*bcn* space group. The energy barrier is predicted to be about 85 meV/f.u. [see Fig. 4(a)], which is much smaller than that (approximately 340 meV/f.u.) obtained with the P*nna* PE structure and even smaller than that of $PbTiO_3$ (approximately 200 meV) [38]. During the switching, the coordination numbers of some Fe sites are changed, and all atoms are displaced within the original sheet. For example, the tetrahedral *D* sublattice and octahedral *A* sublattice in sheet 3 of the FE↓ state transform to the octahedral *A* sublattice and tetrahedral *D* sublattice in sheet 3 of the FE↑ state, respectively. Note that the two sublattices *A* and *D* become equivalent (occupying the octahedral 8*d* Wyckoff position) in the PE state. In contrast, for the P*nna* PE structure, not only do the sublattices change during the switching between the FE↑ state and FE↓ state, but also the

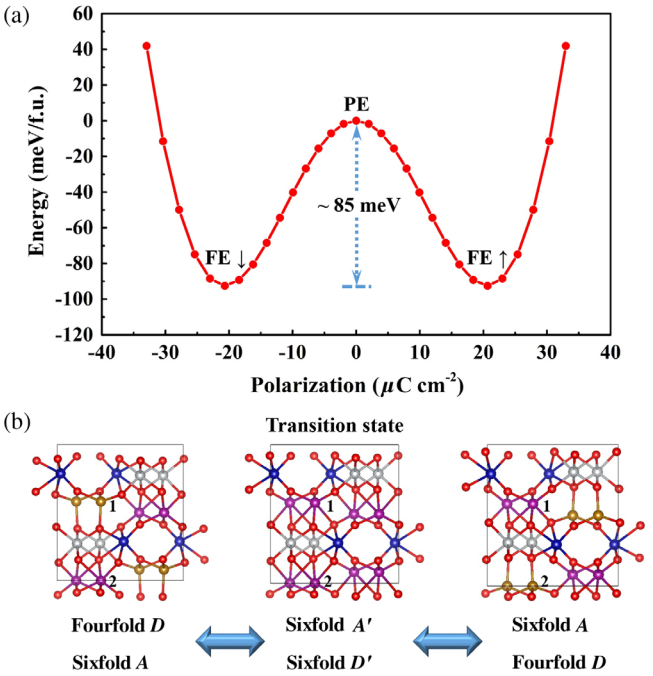

FIG. 4. FE-PE phase transition path in ε-Fe_2O_3 from the SSW simulation. (a) Total energy as a function of the electric polarization shows an energy barrier of 85 meV/f.u. (b) Detailed structural changes during the FE switching. The octahedral *A* sublattice and tetrahedral *D* sublattice are swapped during the FE switching. Note that the two sublattices *A* and *D* become equivalent in the P*bcn* PE transition state.

sheets interchange (see Ref. [21], Fig. S4). The reason why the new P*bcn* PE structure is much more stable than the P*nna* PE structure is twofold: (1) In the P*bcn* PE structure, only the sublattices *A* and *D* change the local environment. In contrast, all four sublattices undergo drastic changes in the P*nna* PE structure. (2) The octahedral Fe ions in the P*bcn* PE structure are in a more favorable environment than that in the P*nna* PE structure with some rather long Fe—O bonds. The stability of two PE structures is confirmed by the bond-valence sum method [39], which shows that the bond valences of the octahedral Fe sites (see Ref. [21], Table S4) in the P*bcn* structure are closer to +3 than the P*nna* structure. In addition, we propose that the P*bcn* PE structure might be also applicable to $GaFeO_3$. Based on the concept of asymmetric multiferroics [40], we propose a switching path for $GaFeO_3$ with much smaller energy barriers (254 and 105 meV/f.u. for the FE↑ state and FE↓ state, respectively) than that (500 meV/f.u.) through the P*nna* PE $GaFeO_3$ structure (see Ref. [21], Fig. S6).

The density-functional-perturbation-theory [41–43] results show that the P$na2_1$ FE structure is stable without any imaginary frequency, while there is an optical branch at the Γ point with $\upsilon = -105$ cm^{-1} for the P*bcn* PE structure. This phonon normal mode with B_{1u} (or, equivalently, Γ_2^-) symmetry will break the inversion symmetry of the P*bcn* PE structure, which reduces the point group symmetry from

D_{2h} to C_{2v}, resulting in a polarization along the z direction. Using the Berry phase approach [44,45], the electric polarization of ε-Fe_2O_3 along z is computed to be 20.66 $\mu C/cm^2$, a similar magnitude as that in $GaFeO_3$ [19].

E. Mechanism of ferroelectricity in ε-Fe_2O_3

Finally, we briefly discuss the origin of ferroelectricity in ε-Fe_2O_3 on the basis of our proposed Pbcn PE structure. The reason why the Pbcn PE structure has a higher energy than the P$na2_1$ FE structure is that the formed FeO_6 octahedron (8d Wyckoff site) is elongated. After the FE transition, the 8d octahedral Fe site in the Pbcn PE structure becomes either a favorable tetrahedral D site or a favorable octahedral A site in the P$na2_1$ FE structure. We propose that the ferroelectricity in ε-Fe_2O_3 is due to the size effect of the Fe^{3+} ion: If the Fe^{3+} ionic radius becomes larger, the 8d octahedral Fe site in the Pbcn PE structure becomes more favorable; otherwise, the FE state becomes even more stable. The FE mechanism of ε-Fe_2O_3 is different from the usual FE mechanism (e.g., in $BaTiO_3$) due to the pseudo-Jahn-Teller effect, where the hybridization between the empty Ti d states and occupied O $2p$ states leads to an energy lowering. Our hypothesis is supported by additional DFT + U calculations. An increase of the Hubbard U value makes the PE state even more unstable, resulting in an increased energy barrier between the FE and PE states. This trend cannot be explained by the pseudo-Jahn-Teller effect, which predicts that the stability of the FE state decreases with U since the band gap increases with U, in disagreement with the DFT + U result. In contrast, the DFT + U result can be naturally explained in terms of the Fe^{3+} ionic radius. An increase of U makes the 3d electrons of the Fe^{3+} ion more localized and, thus, the Fe^{3+} ion radius smaller, which subsequently makes the PE state even more unstable. Therefore, we attribute the mechanism of the ferroelectricity in magnetic ε-Fe_2O_3 to the size effect of the Fe^{3+} ion instead of the pseudo-Jahn-Teller effect.

III. CONCLUSION

In summary, based on the DFT calculations, PTMC simulations, and SSW simulations, we reveal the origin of the room-temperature ferrimagnetism and the robust ferroelectricity in ε-Fe_2O_3. The strong spin frustration in D-sublattice Fe-Fe pairs induces a net ferrimagnetic magnetization. The SSW simulation predicts a low-energy Pbcn PE structure for ε-Fe_2O_3, explaining why the FE polarization is switchable. Our work suggests a direction to search multiferroics in spin-frustrated systems and/or compounds containing ions in different local environments.

ACKNOWLEDGMENTS

This work is supported by National Nature Science Foundation of China (NSFC) (Grant No. 11374056), the Special Funds for Major State Basic Research (Grant No. 2015CB921700), the Program for Professor of Special Appointment (Eastern Scholar), the Qing Nian Ba Jian Program, and the Fok Ying Tung Education Foundation. We thank Yun Xie, Wei Luo, and Yilin Zhang for helpful discussions. K. X. is partially supported by NSFC Grant No. 11404109.

[1] S. W. Cheong and M. Mostovoy, Multiferroics: A magnetic twist for ferroelectricity, Nat. Mater. **6**, 13 (2007).
[2] R. Ramesh and N. Spaldin, Multiferroics: Progress and prospects in thin films, Nat. Mater. **6**, 21 (2007).
[3] J. van den Brink and D. Khomskii, Multiferroicity due to charge ordering, J. Phys. Condens. Matter **20**, 434217 (2008).
[4] S. Picozzi and C. Ederer, First principles studies of multiferroic materials, J. Phys. Condens. Matter **21**, 303201 (2009).
[5] Y. Tokura and S. Seki, Multiferroics with spiral spin orders, Adv. Mater. **22**, 1554 (2010); K. F. Wang, J. M. Liu, and Z. F. Ren, Multiferroicity: The coupling between magnetic and polarization orders, Adv. Phys. **58**, 321 (2009); J. M. Rondinelli and C. J. Fennie, Octahedral rotation-induced ferroelectricity in cation ordered perovskites, Adv. Mater. **24**, 1961 (2012); N. A. Benedek and C. J. Fennie, Hybrid Improper Ferroelectricity: A Mechanism for Controllable Polarization-Magnetization Coupling, Phys. Rev. Lett. **106**, 107204 (2011).
[6] L. C. Gómez-Aguirre, B. Pato-Doldán, J. Mira, S. Castro-García, M. A. Señarís-Rodríguez, M. Sánchez-Andújar, J. Singleton, and V. S. Zapf, Magnetic ordering-induced multiferroic behavior in $[CH_3NH_3][Co(HCOO)_3]$ metal–organic framework, J. Am. Chem. Soc. **138**, 1122 (2016).
[7] M. Dawber, K. M. Rabe, and J. F. Scott, Physics of thin-film ferroelectric oxides, Rev. Mod. Phys. **77**, 1083 (2005).
[8] N. A. Spaldin, S. W. Cheong, and R. Ramesh, Multiferroics: Past, present, and future, Phys. Today **63**, 38 (2010).
[9] H. J. Zhao, W. Ren, Y. Yang, J. Íñiguez, X. M. Chen, and L. Bellaiche, Near room-temperature multiferroic materials with tunable ferromagnetic and electrical properties, Nat. Commun. **5**, 4021 (2014); P. S. Wang, W. Ren, L. Bellaiche, and H. J. Xiang, Predicting a Ferrimagnetic Phase of Zn_2FeOsO_6 with Strong Magnetoelectric Coupling, Phys. Rev. Lett. **114**, 147204 (2015).
[10] I. Sosnowska, T. Peterlin-Neumaier, and E. Steichele, Spiral magnetic ordering in bismuth ferrite, J. Phys. C **15**, 4835 (1982).
[11] M. Gich, I. Fina, A. Morelli, F. Sánchez, M. Alexe, J. Gàzquez, J. Fontcuberta, and A. Roig, Multiferroic iron oxide thin films at room temperature, Adv. Mater. **26**, 4645 (2014).
[12] E. Tronc, C. Chanéac, and J. P. Jolivet, Structural and magnetic characterization of ε-Fe_2O_3, J. Solid State Chem. **139**, 93 (1998).
[13] R. Schrader and G. Büttner, Eine neue Eisen(III)-oxidphase: ε-Fe_2O_3, Z. Anorg. Allg. Chem. **320**, 220 (1963).
[14] I. Dézsi and J. M. D. Coey, Magnetic and thermal properties of ε-Fe_2O_3, Phys. Status Solidi A **15**, 681 (1973).
[15] M. Gich, C. Frontera, A. Roig, E. Taboada, and E. Molins, High- and low-temperature crystal and magnetic structures

of ε-Fe_2O_3 and their correlation to its magnetic properties, Chem. Mater. **18**, 3889 (2006).

[16] N. Shamir and E. Gurewitz, The magnetic structure of $Bi_2Fe_4O_9$—Analysis of neutron diffraction measurements, Acta Crystallogr. Sect. A **34**, 662 (1978).

[17] Z. V. Pchelkina and S. V. Streltsov, *Ab initio* investigation of the exchange interaction in $Bi_2Fe_4O_9$: The Cairo pentagonal lattice compound, Phys. Rev. B **88**, 054424 (2013).

[18] H. Moriwake1, A. Konishi, T. Ogawa, K. Fujimura, C. A. J. Fisher, A. Kuwabara, T. Shimizu, S. Yasui, and M. Itoh, Ferroelectricity in wurtzite structure simple chalcogenide, Appl. Phys. Lett. **104**, 242909 (2014).

[19] S. Mukherjee, A. Roy, S. Auluck, R. Prasad, R. Gupta, and A. Garg, Temperature Nanoscale Ferroelectricity in Magnetoelectric $GaFeO_3$ Epitaxial Thin Films, Phys. Rev. Lett. **111**, 087601 (2013).

[20] S. Song, H. M. Jang, N. S. Lee, J. Y. Son, R. Gupta, A. Garg, J. Ratanapreechachai, and J. F. Scott, Ferroelectric polarization switching with a remarkable high activation energy in orthorhombic $GaFeO_3$ thin films, NPG Asia Mater. **8**, e242 (2016).

[21] See Supplemental Material at http://link.aps.org/supplemental/10.1103/PhysRevApplied.9.044011 for details on the computational methods, energy of all possible 8384 collinear spin configurations, superexchange interactions in ε-Fe_2O_3, P*bcn* and P*nna* PE structures, bond valence sum in the P*bcn* and P*nna* PE structures, and a possible reaction pathway in the $GaFeO_3$, which includes Refs. [22–31].

[22] P. Hohenberg and W. Kohn, Inhomogeneous electron gas, Phys. Rev. **136**, B864 (1964).

[23] P. E. Blöchl, Projector augmented-wave method, Phys. Rev. B **50**, 17953 (1994).

[24] G. Kresse and J. Hafner, *Ab initio* molecular dynamics for liquid metals, Phys. Rev. B **47**, 558 (1993).

[25] G. Kresse and J. Furthmüller, Efficiency of *ab-initio* total energy calculations for metals and semiconductors using a plane-wave basis set, Comput. Mater. Sci. **6**, 15 (1996).

[26] J. P. Perdew, A. Ruzsinszky, G. I. Csonka, O. A. Vydrov, G. E. Scuseria, L. A. Constantin, X. Zhou, and K. Burke, Restoring the Density-Gradient Expansion for Exchange in Solids and Surfaces, Phys. Rev. Lett. **100**, 136406 (2008).

[27] V. I. Anisimov, F. Aryasetiawan, and A. I. Lichtenstein, The Hubbard model on the triangular lattice: A slave-boson study, J. Phys. Condens. Matter **9**, 767 (1997).

[28] H. J. Xiang, E. J. Kan, Su-Huai Wei, M.-H. Whangbo, and X. G. Gong, Predicting the spin-lattice order of frustrated systems from first principles, Phys. Rev. B **84**, 224429 (2011).

[29] H. J. Xiang, C. H. Lee, H.-J. Koo, X. G. Gong, and M.-H. Whangbo, Magnetic properties and energy-mapping analysis, Dalton Trans. **42**, 823 (2013).

[30] Bond valence parameters, International Union of Crystallography, retrieved 2012, https://www.iucr.org/resources/data/datasets/bond-valence-parameters.

[31] T. Arima, D. Higashiyama, Y. Kaneko, J. P. He, T. Goto, S. Miyasaka, T. Kimura, K. Oikawa, T. Kamiyama, R. Kumai, and Y. Tokura, Structural and magnetoelectric properties of $Ga_{2-x}Fe_xO_3$ single crystals grown by a floating-zone method, Phys. Rev. B **70**, 064426 (2004).

[32] J. B. Goodenough, Theory of the role of covalence in the perovskite-type manganites $[La, M(II)]MnO_3$, Phys. Rev. **100**, 564 (1955); J. Kanamori, Super-exchange interaction and symmetry properties of electron orbitals, J. Phys. Chem. Solids **10**, 87 (1959).

[33] T. Kimura, T. Goto, H. Shintani, K. Ishizaka, T. Arima, and Y. Tokura, Magnetic control of ferroelectric polarization, Nature (London) **426**, 55 (2003).

[34] H. Ueda, H. A. Katori, H. Mitamura, T. Goto, and H. Takagi, Magnetic-Field Induced Transition to the 1/2 Magnetization Plateau State in the Geometrically Frustrated Magnet $CdCr_2O_4$, Phys. Rev. Lett. **94**, 047202 (2005).

[35] D. Stoeffler, First principles study of the electric polarization and of its switching in the multiferroic $GaFeO_3$ system, J. Phys. Condens. Matter **24**, 185502 (2012).

[36] S. C. Zhu, S. H. Xie, and Z. P. Liu, Nature of rutile nuclei in anatase-to-rutile phase transition, J. Am. Chem. Soc. **137**, 11532 (2015).

[37] Y. F. Li, S. C. Zhu, and Z. P. Liu, Reaction network of layer-to-tunnel transition of MnO_2, J. Am. Chem. Soc. **138**, 5371 (2016).

[38] R. E. Cohen, Origin of ferroelectricity in perovskite oxide, Science **358**, 136 (1992).

[39] C. Preiser, J. Lösel, I. D. Brown, M. Kunz, and A. Skowron, Long range Coulomb forces and localized bonds, Acta Crystallogr. Sect. B **55**, 698 (1999).

[40] X. Z. Lu and H. J. Xiang, Designing asymmetric multiferroics with strong magnetoelectric coupling, Phys. Rev. B **90**, 104409 (2014).

[41] S. Baroni, S. De Gironcoli, A. Dal Corso, and P. Giannozzi, Phonons and related crystal properties from density-functional perturbation theory, Rev. Mod. Phys. **73**, 515 (2001).

[42] X. Gonze, First-principles responses of solids to atomic displacements and homogeneous electric fields: Implementation of a conjugate-gradient algorithm, Phys. Rev. B **55**, 10337 (1997).

[43] X. Gonze and C. Lee, Dynamical matrices, Born effective charges, dielectric permittivity tensors, and interatomic force constants from density-functional perturbation theory, Phys. Rev. B **55**, 10355 (1997).

[44] R. D. King-Smith and D. Vanderbilt, Theory of polarization of crystalline solids, Phys. Rev. B **47**, R1651 (1993).

[45] R. Resta, Macroscopic polarization in crystalline dielectrics: The geometric phase approach, Rev. Mod. Phys. **66**, 899 (1994).